

## **ACKNOWLEDGEMENTS:**

I would like to thank my committee for their continued support and commitment to my success. A very special thank you goes to Amanda Dye for her invaluable support with the day-to-day tasks of this study. I would also like to thank others who contributed to the success of this study: Dr. James McClure, Morgan Talley, and Blythe Carter.

This work was supported by:

National Science Foundation Grant 0941235

Department of Energy Grant DE-SC0002163,

National Institute of Environmental Health Sciences Grant P42 ES05948.

I am truly grateful for the support I've received throughout this project; I could not have done it on alone.

## TABLE OF CONTENTS:

List of Tables .....	4
List of Figures .....	4
Abstract .....	5
Introduction.....	5
Materials and Methods.....	7
Results .....	12
Discussion.....	24
References.....	28

## **LIST OF TABLES**

Table 1. Number of DNRs observed relative to total number of DNRs.

Table 2. Average SSACR and orientation in flow for aggregate DNR system throughout dissolution.

Table 3. Average volume, surface areas and parameterized surface areas for aggregate DNR system throughout dissolution.

Table 4. Morphological characteristic of Reeves throughout dissolution.

Table 5. Morphological characteristic of Ian throughout dissolution.

Table 6. Volume, SSACR, surface areas and parameterized surface areas for DNRs in the Remain and Dissolve groups.

## **LIST OF FIGURES**

Figure 1. Visualized X-ray transmission values for a cross-section of the column using beam energies above the cesium K-edge (a), between the iodine K-edge and the cesium K-edge (b) and below the iodine K-edge (c).

Figure 2. Histograms of mesh (X-ray transmission) values associated with using beam energies above the cesium K-edge (a), between the iodine K-edge and the cesium K-edge (b) and below the iodine K-edge (c).

Figure 3. Individual and median volume throughout dissolution of DNRs that remained in the second dissolution step.

Figure 4. Individual and median DNR SSACR throughout dissolution for DNRs that remained in the second dissolution step

Figure 5. Wetting-nonwetting intrinsic surface area of DNRs that remained after two dissolution steps

Figure 6. Conceptual diagram for the classification of DNRs into Dissolve and Remain groups.

**ABSTRACT:**

Organic immiscible fluids are common subsurface contaminants which may leach into the groundwater supply, posing a threat to human health. The development of effective remediation techniques is dependent upon a thorough understanding of the microscale processes that govern the dissolution of non-aqueous phase liquid (NAPL). In order to resolve the local mass transfer in the dissolution process from a fundamental perspective, both the pore-space and NAPL morphology must be known. The purpose of this study was to assess the morphology of trapped NAPL during dissolution using three-dimensional (3-D) image analysis. Data was taken from a previous experiment where a column was packed with a representative porous medium and trichloroethylene (TCE), and flushed with a solution containing hydroxypropyl- $\beta$ -cyclodextrin (Schnaar and Brusseau 2006). 3-D images were taken of the column in its residual state and after each successive flush using X-ray microtomography. Image analysis was performed to assess the orientation, curvature, volume, and surface area of the NAPL. A comparison was constructed between the disconnected NAPL regions (DNRs) that were flushed and those that persisted. The volume, roundedness and orientation were important determinants of dissolution.

**INTRODUCTION:**

NAPLs including chlorinated solvents, fuel oils and gasoline products are common subsurface contaminants. These compounds, often released into the environment by industrial processes, may become trapped in the subsurface due to capillary forces. Trapped NAPLs slowly dissolve over time, creating a long-term source of pollution for the drinking water supply. Many organic fluids, including TCE, the model NAPL used in this study, are known or probable

carcinogens. As such, their presence in the drinking water supply is a significant threat to human health.

To assess the risk posed by trapped NAPL to groundwater resources, its dissolution behavior must be understood. In the microscale, dissolution is governed by the mass transfer between the NAPL and the aqueous phase. Models commonly characterize the mass transfer between the non-aqueous and aqueous phases as being proportional to the product of the deviation of the aqueous phase concentration of the dissolved NAPL from equilibrium (Miller et. al 1990). However, accurate representations of NAPL morphology and the NAPL-aqueous interface are typically not accessible quantities (Khachikian and Harmon 2000). By constructing a better understanding of trapped NAPL morphology, the ability to predict NAPL dissolution will be improved.

There have been numerous previous attempts to characterize NAPL morphology during dissolution. Early studies relied on styrene polymerization of NAPL bodies to quantify their shape and size (e.g. Powers et. al. 1994). The inherent disadvantage of this study design is that it is invasive; each phase is separated to recover the polymerized NAPL. This feature makes it difficult to assess changes to NAPL throughout the dissolution process (Khachikian and Harmon 2000). Other studies have relied on two-dimensional micromodels to characterize NAPL morphology (e.g. Corapcioglu et. al. 2009). These studies assess the behavior of NAPL within an artificial, transparent network of interconnecting pores and throats (Corapcioglu et. al. 2009).

Advances in 3-D imaging technologies have furthered our ability to study NAPL dissolution. The non-invasive nature of 3-D imaging allows for the assessment of changes to the morphology of an individual NAPL region (DNR) throughout dissolution. Previous studies have used magnetic resonance imaging (MRI) to study NAPL morphology, particularly the surface

area-to-volume ratio (Johns and Gladden 2000). However, due to limitations in resolving the phases within the image taken by MRI, the study used 1mm ballotini as the representative porous media, where the grain size of natural soils ranges from 0.25 mm to 1.0 mm (Johns and Gladden 2001). Another study, conducted by Zhang et. al. used synchrotron X-ray microtomography to directly quantify NAPL size and geometry (2002). However, due to poor resolution, the study was unable to identify DNRs in isolation; instead, investigators relied on integrated measures of all DNRs within their experiment (Zhang et. al. 2002).

The current study uses images taken from a previous study performed by Schnaar and Brusseau (2006). The current study resolved the images and analyzed them for the following parameters: volume, curvature, orientation, and interfacial surface area.

## **MATERIALS AND METHODS**

TCE was used as the model NAPL for this study. The TCE was doped with iodobenzene (8% by volume) to enhance image contrast. The aqueous phase was doped with cesium chloride (60 g/L). Commercially available 45/50 Accusand (Accusand, Unimin Co.) was used as the representative porous medium. The median grain size of the media was 0.35mm. The uniformity coefficient ( $U = d_{60}/d_{10}$ ;  $d_i$  is the  $i$ th percentile of grains by mass that are smaller than a given sieve size) of the media was 1.0.

### **Establishment of Organic-Liquid Saturation and Column Flushing**

As described by Schnaar and Brusseau (2006), the porous medium was dry-packed into a thin-walled, X-ray transparent column made of aluminum, with Swagelok end-fittings. The column was 4.4 cm long, with an inner diameter of 0.58 cm. Glass inserts (1.4 cm long, 0.2 cm in diameter) were placed at the ends of the column. Polypropylene frits (10- $\mu$ m pores) were placed between the glass inserts and the porous media. As a result of these additions, the total

length of the porous medium zone was approximately 1.5 cm. The equivalent of 5 pore-volumes ( $\sim 1 \text{ cm}^3$ ) of TCE was then pumped vertically upward into the column using a syringe pump (Sage). An aqueous solution containing TCE and iodobenzene was then flushed vertically downward at 20 cm/hr to displace the organic liquid.

As discussed by Schnaar and Brusseau (2006), the column was then sealed and imaged as described below. After the first, “residual” scan, the column was flushed with an aqueous solution at a Darcy velocity of 17 cm/hr. To increase the solubility of the organic liquid in the aqueous phase, the flushing solution contained hydroxypropyl- $\beta$ -cyclodextrin (HPCD, 5 wt %).

During each dissolution step, approximately 65 pore volumes of the HPCD solution were flushed through the column. Following this, approximately 10 additional pore volumes of solution containing no HPCD and 60 g/L cesium chloride were flushed through the column to introduce the aqueous-phase dopant. The column flushing procedure was implemented three times on the column. The column was sealed and imaged following each dissolution step.

### **Synchrotron X-ray micro-tomography**

3-D images were taken of the column in its residual state and after each dissolution step. Imaging was performed at the GeoSoilEnviroCARS BM-13D Beamline at the Advanced Photon Source at Argonne National Laboratory, Illinois. The imaged zone spanned the entire length of the porous medium zone within the column. Two beams of different energies were used to resolve each of the three phases. Images were collected above and below the iodine K-edge (33.0169 and 33.269 keV) to resolve the non-aqueous phase, and below and above the cesium K-edge (33.279 and 36.085 keV) to resolve the aqueous phase. Spatial resolution of the images was approximately  $11 \mu\text{m}$ , and the images had a resolution of  $580 \times 580 \times 1050$ .

## **Resolving the image and data processing**

The raw data from the imaging process consisted of three, 3-D meshes, with each mesh corresponding to one of the energy levels used in the X-ray micro-tomography: below the iodine K-edge, between the iodine K-edge and the cesium K-edge and above the cesium K-edge. Mesh values were the X-ray transmission for a given point within the column. Cross-sections of the visualized meshes are displayed in Figure 1.

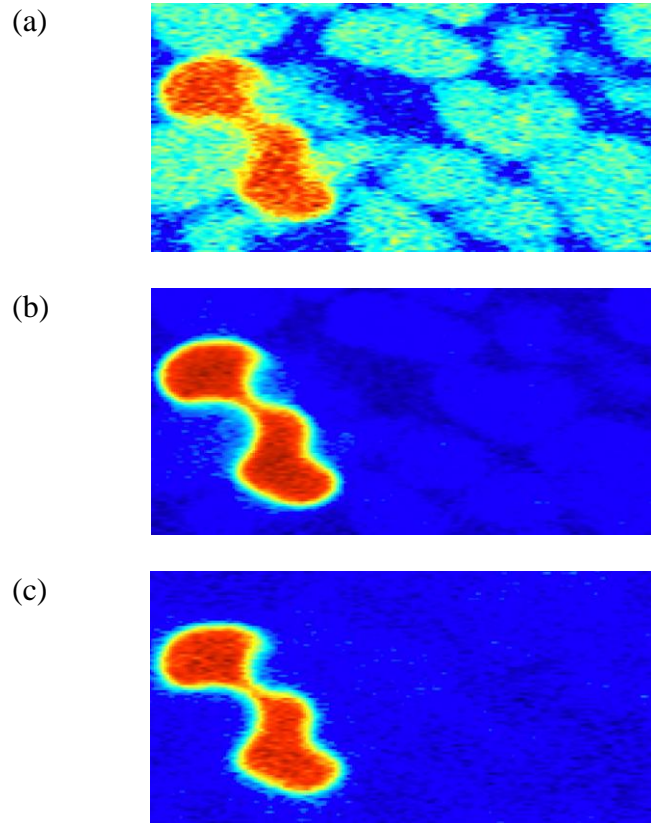


Figure 1. Visualized X-ray transmission values for a cross-section of the column using beam energies above the cesium K-edge (a), between the iodine K-edge and the cesium K-edge (b) and below the iodine K-edge (c).

The goal of image processing was to construct a composite image from the three meshes where the solid, non-aqueous and aqueous phases were each well-resolved. The raw image constructed by the meshes yielded poor separation between the phases, making it difficult to identify interfaces (Figure 1). The meshes were processed to enhance the resolution of the phases, and thus enable the study of interfacial area. First, the meshes were subjected to a modified Gaussian filtering algorithm to remove noise from the histogram of X-ray transmission values. Each phase was assumed to have a normal distribution. For transmission values that were located within overlapping phase distributions, the probability of transmission value belonging to a given phase was calculated, and the value was classified accordingly. Next the X-

ray transmission values associated with each interface was identified. Figure 2 shows a histogram of the X-ray transmission values for the mesh for each energy beam used during micro-tomography. The greatest, middle and smallest peaks of the histogram correspond to the X-ray transmission values associated with the solid, aqueous and non-aqueous phases, respectively (Figure 2). An isovalue mask was applied to the mesh and the enclosed area was cropped. The value of the mask was chosen to be the average transmission between the peaks on the histogram. This value is the transmission level associated with the interface between any two phases.

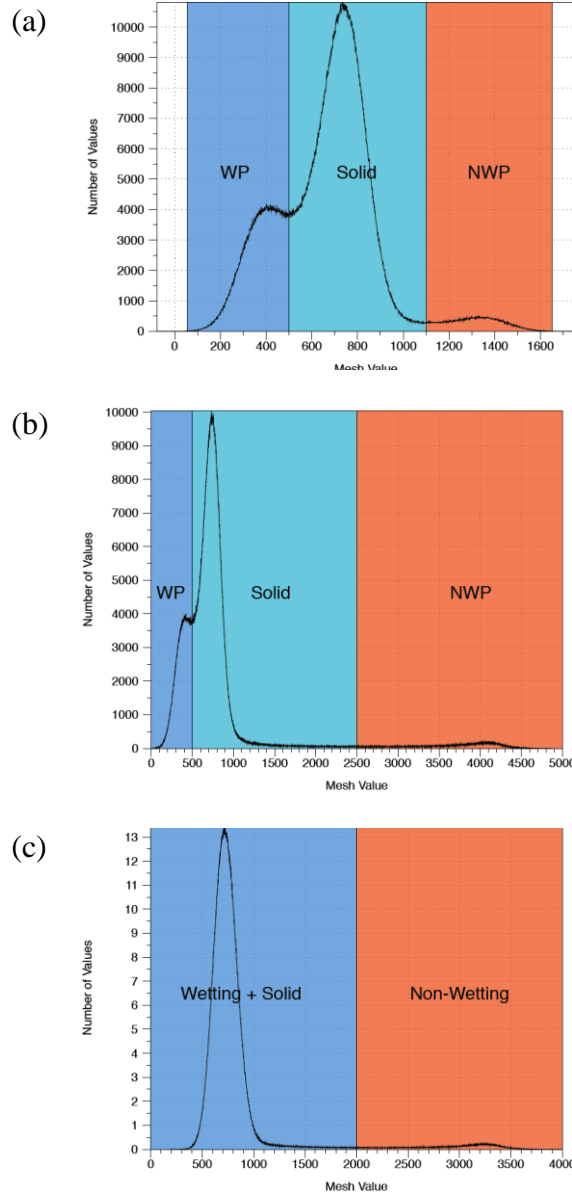


Figure 2. Histograms of mesh (X-ray transmission) values associated with using beam energies above the cesium K-edge (a), between the iodine K-edge and the cesium K-edge (b) and below the iodine K-edge (c).

Once the interfaces were rendered sufficiently smooth, the images were analyzed using the image processing software DataTank, which is available online from <http://www.visualdatatools.com/DataTank/index.html>. DataTank assessed the NAPL for the following parameters: curvature, orientation, interfacial surface area, and volume. This analysis

will rely on terminology commonly used in describing multiphase flow. The NAPL may hereafter be referred to as the nonwetting (N) phase, the aqueous solution may be described as the wetting (W) phase, and the solid may be referred to as the solid (S) phase

DNR orientation was quantified by the orientation tensor. At each point on the interface, the orientation was calculated as the dyadic product of the normal vector. These values were then averaged over both the nonwetting-wetting (NW) and nonwetting-solid (NS) interfaces to generate the reported values. This analysis focuses on the  $G_{zz}$  value for the NW interface, as it was observed to have the greatest changes throughout dissolution, and the aqueous solution was flushed in the vertical, z-direction.

It was hypothesized that the DNR would become more rounded throughout dissolution. This morphological change was quantified by the unitless parameter of the specific surface area-to-curvature ratio (SSACR). By comparing the SSACR of a given DNR to the SSACR of a sphere, one can deduce the overall roundedness of a NAPL feature. The curvature,  $J$ , was calculated as the divergence of the normal vector at a given point ( $m^{-1}$ ). This value was averaged over the entire DNR surface, generating an average curvature. The specific surface area (SSA) was calculated as the surface area to volume ratio ( $m^2m^{-3}$ ). These values are defined mathematically as follows:

$$J = \nabla \cdot \bar{n} = \frac{\partial n_x}{\partial x} + \frac{\partial n_y}{\partial y} + \frac{\partial n_z}{\partial z}$$

For a sphere,  $J$  can be simplified to

$$J = \frac{2}{R}$$

where  $R$  is the radius of the sphere. SSA for a sphere is

$$SSA = \frac{\text{Surface Area}}{\text{Volume}} = \frac{4\pi R^2}{\frac{4}{3}\pi R^3} = \frac{3}{R}$$

Finally, the SSACR is the ratio of the SSA to the curvature is equal to

$$SSACR = \frac{SSA}{J} = \frac{3}{2}$$

Thus, the overall roundedness of a DNR can be quantified by comparing its SSACR to that of a sphere, or 1.5. The final value used in this analysis is the specific interfacial area (SIA), or the ratio of the surface area of the NW interface to the total volume. This value describes the contact of each DNR with the wetting fluid relative to its total volume.

## **RESULTS**

This results section consists of three types of analysis. First, the aggregate system of all DNRs is assessed throughout each dissolution step. Second, the DNRs that remained after two dissolution steps are examined to assess changes to their morphology throughout dissolution. Finally, a comparison was constructed between DNRs that dissolved and DNRs that remained entrapped. This comparison allows for the identification of morphological characteristics shared by DNRs that are dissolved.

### **Aggregate System**

The DNRs observed in this study were a subset of all DNRs in the column (Table 1). Some of the DNRs were in contact with the column wall and are considered separately for portions of this analysis. Contact with the column wall may influence the dissolution behavior, and thus, DNRs located on the column wall may not be representative of NAPL within a natural system.

Table 1. Number of DNRs observed relative to total number of DNRs

	Total <sup>1</sup>	Observed	Percentage of total
Residual	285	112	39.2
Dissolution Step 1	267	80	31.2
Dissolution Step 2	66	22	33.3

Changes to the average orientation of the interface in the direction of flow, the NW *Gzz*, were observed. The NW interface tended to be less oriented in the direction of flow for the residual and the second dissolution step, but more oriented in the direction of flow for the first dissolution step (Table 2). While the NW interface for DNRs along the column wall tended to be more oriented in the direction of flow, they observed the same trend as the interior DNRs.

NAPL SSACR increased during each dissolution step.

Table 2. SSACR and NW *Gzz* for aggregate DNR system throughout dissolution.

	Residual	Dissolution Step 1	Dissolution Step 2
<b>SSACR</b>	1.96	5.85	6.84
On wall	2.14	6.94	7.03
Interior	1.81	4.25	6.73
<b>NW <i>Gzz</i></b>	0.289	0.311	0.267
On wall	0.298	0.320	0.277
Interior	0.277	0.299	0.262

The average volume of the DNRs decreased between the residual and the first dissolution step, but increased between the first and second dissolution steps (Table 3). The DNRs on the column wall had a larger average volume than the DNRs on the interior, but followed the same trend. The average NW interfacial area increased throughout dissolution, while the average NS interfacial area decreased slightly in the first dissolution step and increased in the second dissolution step (Table 3). SIA increased throughout dissolution (Table 3).

<sup>1</sup> Calculated by Schnaar and Brusseau 2006

Table 3. Average volume, surface areas and parameterized surface areas for aggregate DNR system throughout dissolution.

	<b>Residual</b>	<b>Dissolution Step 1</b>	<b>Dissolution Step 2</b>
<b>Volume (m<sup>3</sup>)</b>	6.48E-11	5.50E-11	7.88E-11
On wall	7.33E-11	6.00E-11	1.40E-10
Interior	5.22E-11	4.75E-11	5.02E-11
<b>NW Interfacial Area (m<sup>2</sup>)</b>	6.28E-08	1.32E-07	2.40E-07
On wall	6.45E-08	1.32E-07	4.55E-07
Interior	6.04E-08	1.31E-07	1.39E-07
<b>NS Interfacial Area (m<sup>2</sup>)</b>	7.80E-07	5.34E-07	5.38E-07
On wall	7.79E-07	4.79E-07	7.35E-07
Interior	7.82E-07	6.17E-07	4.47E-07
<b>SIA (m<sup>-1</sup>)</b>	9.70E2	2.40E3	3.04E3
On wall	8.80E2	2.20E3	3.25E3
Interior	1.16E3	2.77E3	2.77E3

### **Changes to individual DNR morphology throughout dissolution**

Changes in the morphology of an individual DNR throughout dissolution were assessed. In this section, DNRs may be referred to by their identifying handle. Of the 112 DNRs selected in the residual, 19 remained after the second dissolution step. Two DNRs, Reeves and Apollo, were partially dissolved during the second dissolution step, breaking into smaller DNRs. These DNRs were assessed as independent features, denoted by Roman numerals (e.g. Apollo I, Apollo II). From the 19 parent DNRs and 3 newly isolated DNRs from Reeves and Apollo, there were a total of 22 DNRs assessed in this section.

DNRs tended to decrease in volume throughout dissolution. Figure 3 displays the volume for individual DNR during the three dissolution steps. Additionally, the median DNR volume is shown, indicating the general trend of decreasing volume. DNR volume decreased more dramatically between the first and second dissolution steps. Volume had a greater variance in each dissolution step, indicative of the fact that DNRs did not dissolve at the same rate.

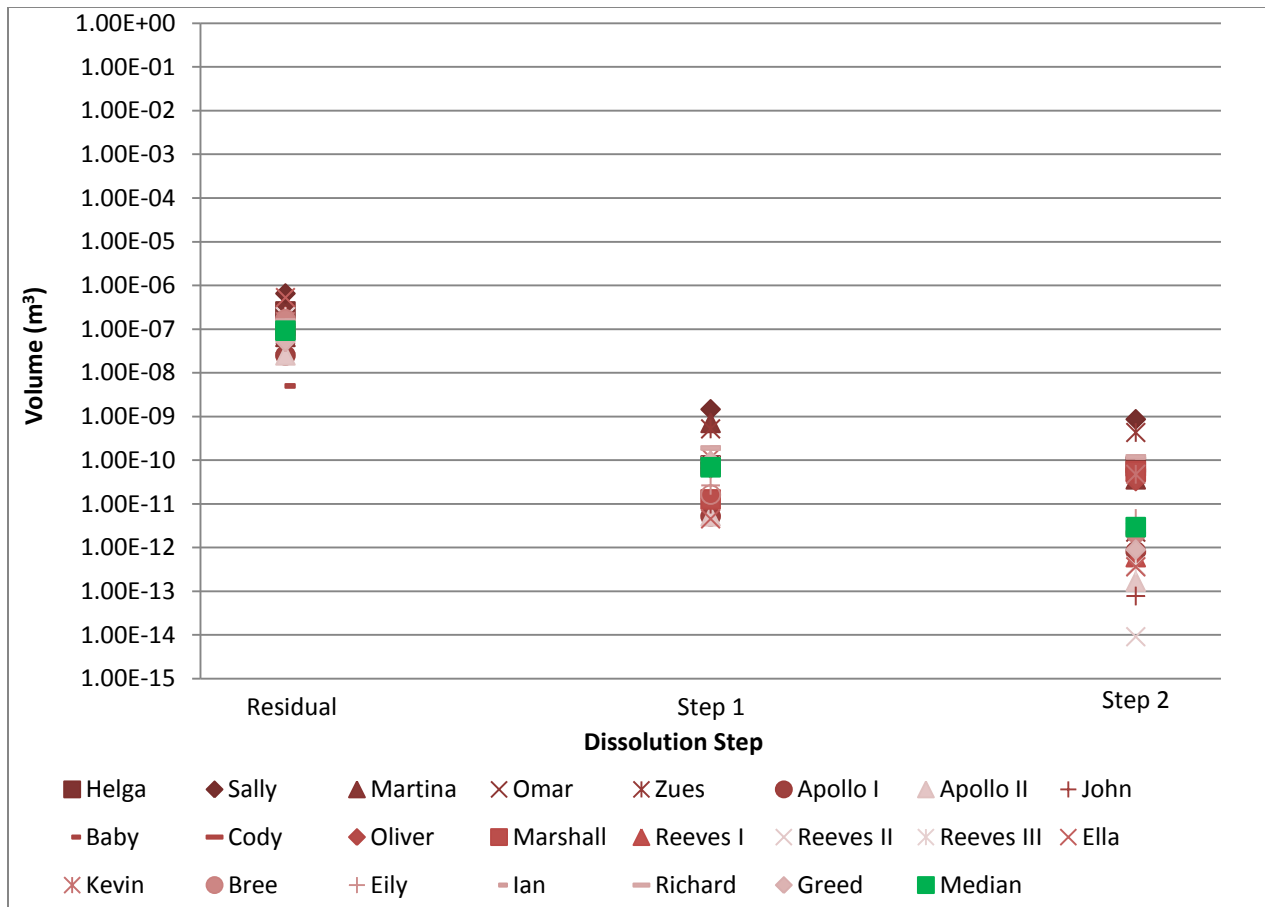


Figure 3. Individual and median volume throughout dissolution for DNRs that remained in the second dissolution step.

The overall roundedness of a DNR, the SSACR was assessed during each dissolution step. SSACR generally increased throughout dissolution, deviating from the SSACR of a sphere. Figure 4 illustrates the changes observed in each DNR, as well as the median value.

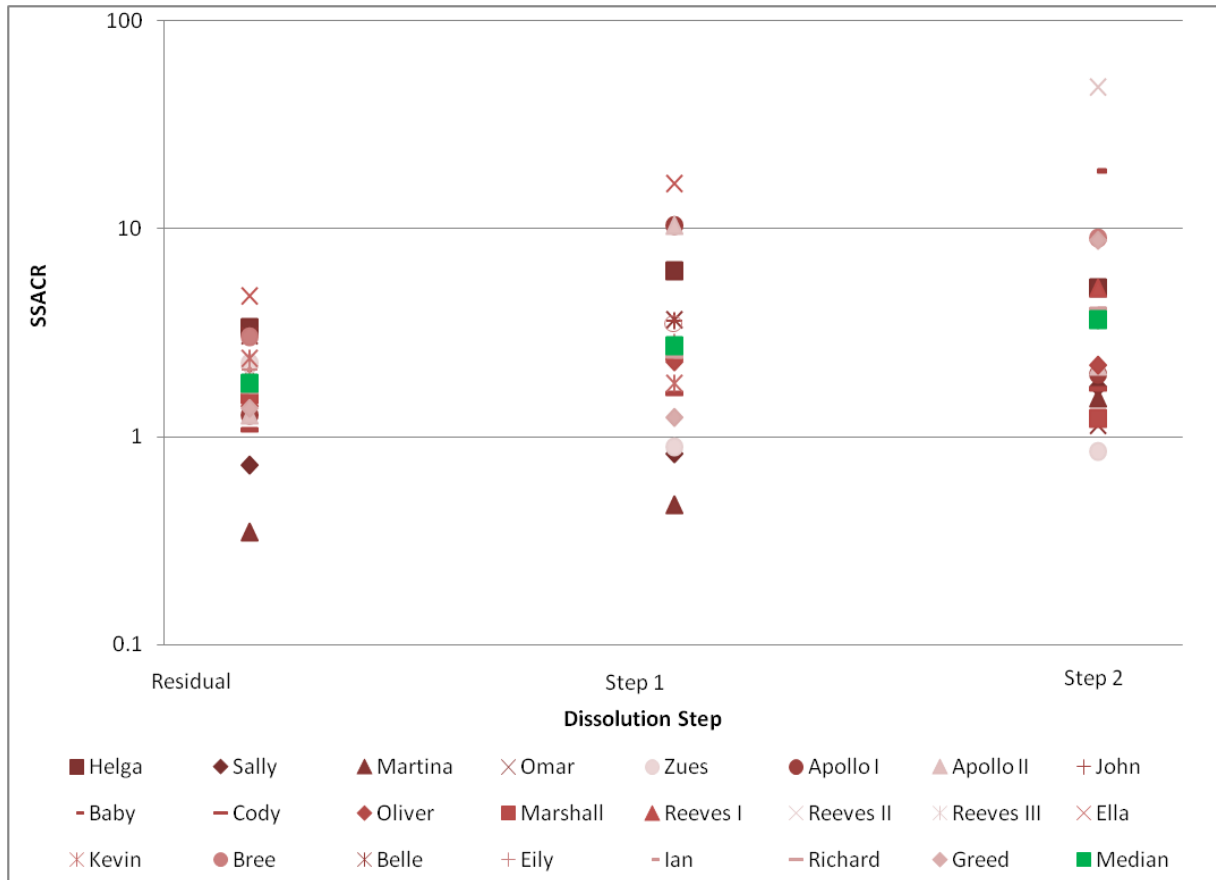


Figure 4. Individual and median SSACR throughout dissolution for DNRs that remained in the second dissolution step.

Generally, SIA increased throughout dissolution, but an increased variance was also observed (Figure 5). To explore this notion, two DNRs, Reeves and Ian, will be examined as case studies.

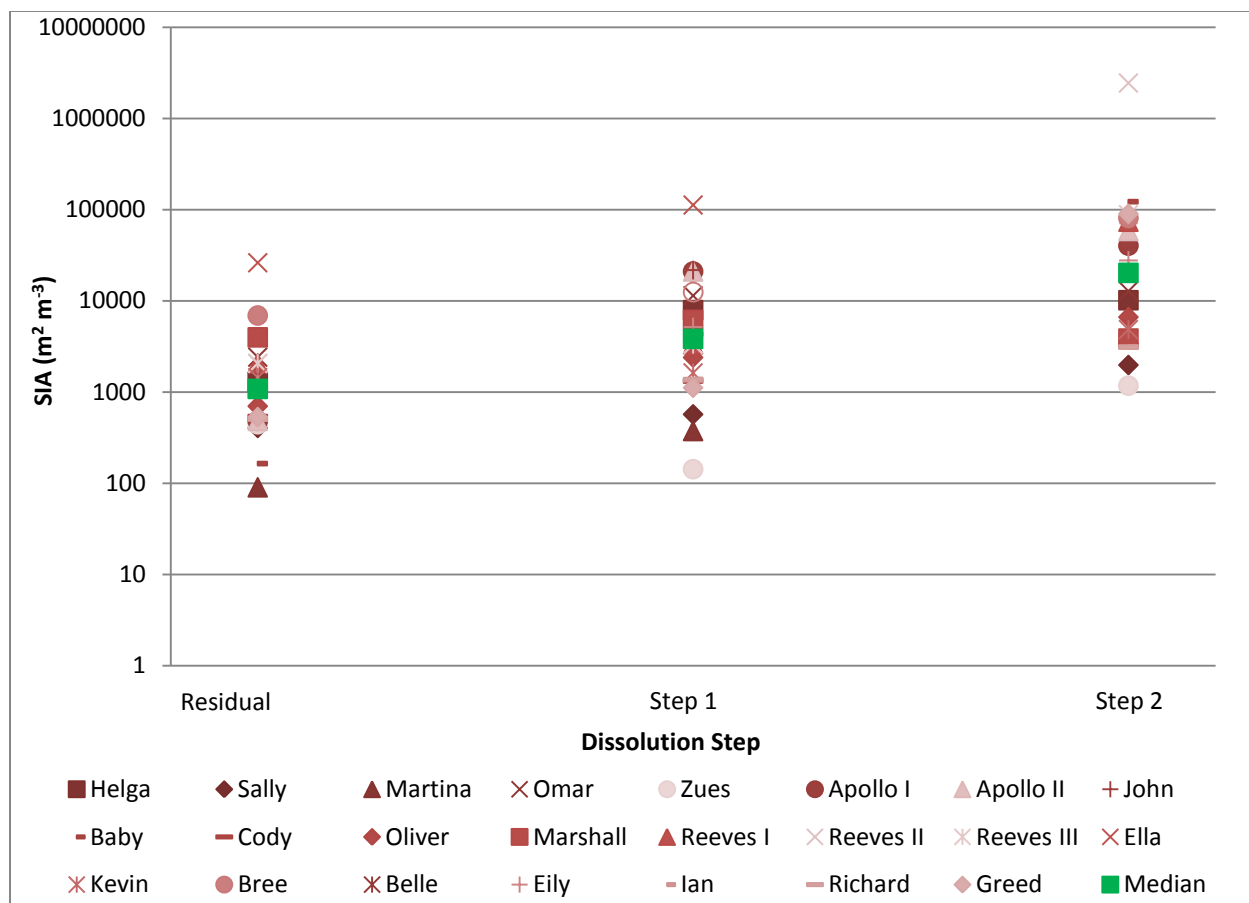
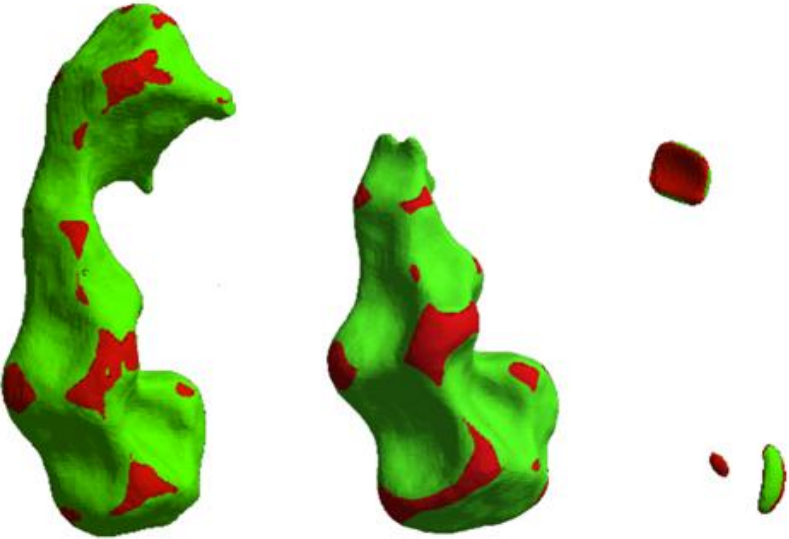


Figure 5. SIA dissolution of the DNRs that remained after two dissolution steps<sup>2</sup>

Reeves was a large DNR located on the column wall. Morphological characteristics for Reeves are summarized in Table 4. In the first dissolution step, the volume decreased as a large lobe of the DNR was dissolved. In the second dissolution step, Reeves was almost entirely dissolved, leaving three small, isolated features (Reeves I, Reeves II and Reeves III). Reeves exhibited an increase in SIA between the residual and first dissolution step and a dramatic increase in SIA was observed between the first and second dissolution steps. Reeves’s SSACR increased throughout dissolution.

<sup>2</sup> A small DNR, Belle, was excluded from this analysis because it had zero NW interfacial area during all three dissolution steps.

Table 4. Morphological characteristic of Reeves throughout dissolution.<sup>3</sup>

	Residual	Dissolution Step 1	Dissolution Step 2
Image <sup>4</sup>			
NW Gzz	0.220	0.124	Reeves I: 0.142 Reeves II: 0.124 Reeves III: 0.107
Volume (m <sup>3</sup> )	9.41 E -11	7.23 E -11	Reeves I: 6.05 E -13 Reeves II: 9.14 E -15 Reeves III: 3.81 E -13
SSACR	1.96	2.71	Reeves I: 5.17 Reeves II: 48.3 Reeves III: 3.76
NW Interfacial area (m <sup>2</sup> )	1.94 E -07	2.41 E -07	Reeves I: 4.46 E -08 Reeves II: 2.23 E -08 Reeves III: 3.36 E -08
NS Interfacial Area (m <sup>2</sup> )	1.64 E -06	1.24 E -06	Reeves I: 3.22 E -08 Reeves II: 5.78 E -10 Reeves III: 1.74 E -08
SIA (m <sup>-1</sup> )	2.06 E 03	3.34 E 03	Reeves I: 7.37 E 04 Reeves II: 2.44 E 06 Reeves III: 8.81 E 04

Ian was a medium-sized DNR located in the interior of the column. During the first dissolution step, the volume of Ian decreased slightly. Additionally, Ian became more rounded,

<sup>3</sup> Reeves I, II and III correspond to the top, lower left, and lower right features, respectively.

<sup>4</sup> Red represents the NW interface, and green represents the NS interface.

as reflected by SSACR approaching 1.5 (Table 5). The volume of Ian decreased by an order of magnitude in the second dissolution step. Also during that step, there was a dramatic increase in NW interfacial area, and consequently SIA. The dissolution pattern of Ian is representative of many of the DNRs observed. Early in dissolution, many DNRs appear to become more spherical and experienced only minor changes to volume. Then, the DNRs would experience a sharp decrease in volume and their geometry changed significantly; changes appear to be dependent on NAPL contact with mobile wetting fluid.

Table 5. Morphological characteristics of Ian throughout dissolution.

	Residual	Dissolution Step 1	Dissolution Step 2
Image			
NW Gzz	0.239	0.264	0.222
Volume (m <sup>3</sup> )	3.50E-11	3.07E-11	3.62E-12
SSACR	3.41	3.00	11.6
NW Interfacial area (m <sup>2</sup> )	1.64E-07	3.39E-07	2.91E-07
NS Interfacial Area (m <sup>2</sup> )	8.72E-07	4.92E-07	1.10E-07
SIA (m <sup>-1</sup> )	4.68 E 03	1.10 E 04	8.04 E 04

### Comparison of lasting and dissolving DNRs

By constructing a comparison of DNRs that last and DNRs that dissolve, important characteristics of dissolution may be observed. For each dissolution step, the DNRs that were fully dissolved were identified. The characteristics of a dissolved DNR were determined for the last dissolution step in which it was present. These values were used to calculate characteristics

of the “dissolved” group. If a DNR persisted into a subsequent dissolution step, the characteristics of that DNR from the preceding dissolution step were used in calculating the features of the “remain” group. This classification process is presented pictorially in Figure 6.

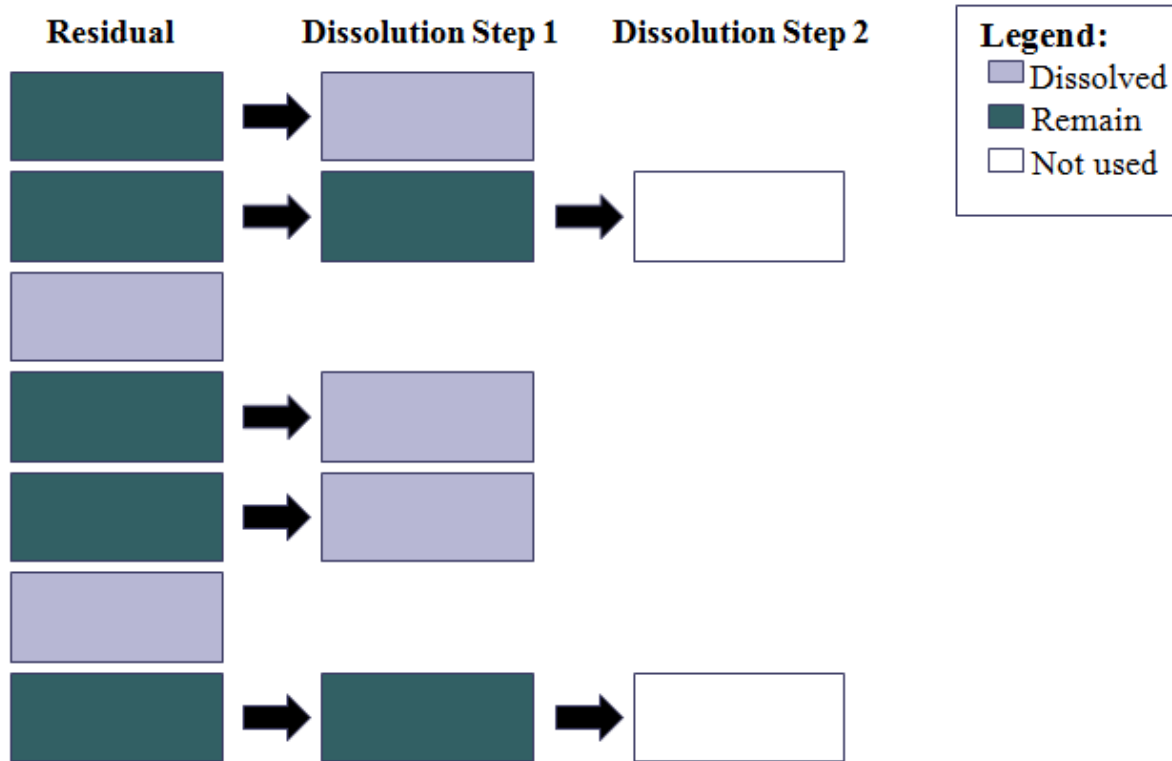


Figure 6. Conceptual diagram for the classification of DNRs into dissolve and remain groups. Each box represents the volume, curvature, and surface area associated with an individual DNR in a given dissolution step.

The average orientation, volume, SIA, surface areas and parameterized surface areas for the dissolved and the remaining DNRs are summarized in Table 6. First, DNRs that dissolved tended to have their NW interface less oriented in the direction of flow than their counterparts that remained. On average, dissolved DNRs were an order of magnitude smaller than DNRs that remained. The SSACR was closer to 1.5 for the dissolve group, indicating that blobs that are more spherical are more likely to dissolve. The SIA was greater for DNRs that dissolved, which

is indicative of the fact that dissolved DNRs had a greater contact with the wetting phase relative to their volume.

Table 6. Orientation, volume, SSACR, surface areas and SIA for DNRs in the remain and dissolve groups.

	<b>Dissolve</b>	<b>Remain</b>
NW $G_{zz}$	0.312	0.287
Volume ( $m^3$ )	1.29E-11	1.01E-10
SSACR	1.48	1.25
NW Interfacial Area ( $m^2$ )	7.01E-08	1.09E-07
NS Interfacial Area ( $m^2$ )	1.82 E 3	8.49 E 03
SIA ( $m^{-1}$ )	1.75E4	1.05 E4

## DISCUSSION AND CONCLUSION

The current study furthers the scientific understanding of NAPL morphology during dissolution. Orientation of the NW interface in the direction of flow was observed to be an important determinant of dissolution. DNRs that dissolved tended to have NW interfaces that aligned perpendicular to the direction of flow. A NW interface that is aligned with the vertical direction is likely to have less efficient contact with aqueous phase.

DNRs tended to become less spherical throughout dissolution. This can be attributed to the fact that many of the smaller blobs, with SSACRs that were close to 1.5 tended to dissolve early. This finding is echoed by the differences between the dissolve and remain groups. More spherical DNR, overall, were more likely to dissolve.

Another important parameter assessed in the current study was volume. A decrease in NAPL volume was anticipated because mass is transferred to the aqueous phase. In the aggregate system, average volume increased between the residual and the first dissolution step. At first glance, this finding may seem surprising, given that one would not expect an increase in NAPL volume during the dissolution process. However, this increase can be attributed to the complete

dissolution of smaller features between residual and the first dissolution step, creating an average volume that is greater in the first dissolution step. DNRs that dissolved tended to have smaller volume than DNRs that remained.

The characterization of the NW interface may prove especially useful, as it may improve our ability to model the mass transfer of NAPL fluid to the aqueous phase. An increase in SIA was predicted due to the confluence of two changing parameters. First, the NAPL volume decreased throughout dissolution. Second, the NW interfacial area increased throughout dissolution. Generally, the wetting fluid infiltrates a pore body through a pore throat, increasing the NW interfacial area. However, decreases in SIA may also be observed, particularly if a DNR is distributed in multiple pore spaces connected by a narrow pore throat. If one of the lobes of the DNR was to dissolve completely, the overall NW interfacial area could decrease. Of these two possible phenomena, the former was more common in the DNRs observed, as indicated by the increase in NW interfacial area exhibited by most DNRs. As observed in all three analyses, SIA increased throughout dissolution.

The current study was subject to a few important limitations. Most importantly, memory restrictions for the image processing software, DataTank, would not allow for the processing of larger NAPL features. This restricted the current study to a subset of smaller DNRs within the column. Large features contained major portions of the total NAPL volume, so their exclusion from this study diminishes the utility of findings presented. However, qualitative observation of the larger DNRs indicates that their dissolution behavior is similar to that of the DNR Reeves. The large features excluded from study tended to be dissolved into smaller, disconnected features. If the memory capabilities of DataTank were improved, future studies could analyze the dissolution behavior of larger NAPL features.

Another limitation of the current study is that NAPL morphology was only studied during three points in dissolution. The kinetics of NAPL dissolution is an important area for study, but it was difficult to assess the how an individual DNR changed throughout dissolution due to the limited available images. X-ray micro-tomography is both an expensive and time-consuming endeavor, so it may not currently be feasible to produce significantly more images. However, if 3-D imaging technologies continue to progress, the cost of imaging could be reduced. A future study could take images more frequently throughout dissolution to detect smaller changes to a DNR during dissolution.

## REFERENCES:

- Corapcioglu MY, Yoon S, Chowdhury S. 2002. Pore-scale analysis of NAPL blob dissolution and mobilization in porous media. *Transp Porous Med.* 79: 419-442.
- Flannery BP, Deckman HW, Roberge WG, Damico KL. 1987. 3-Dimensional X-ray microtomography. *Science.* 237(4821): 1439-1444.
- Johns ML, Gladden LF. 1999. Magnetic resonance imaging study of the dissolution kinetics of octanol in porous media. *Journal of Colloid and Interface Science* 210: 261-270.
- Johns ML, Gladden LF. 2001. Surface-to-volume ratio of ganglia trapped in small-pore systems determined by pulsed-field gradient nuclear magnetic resonance. *Journal of Colloid and Interface Science* 238:96-104.
- Kachikian C, Harmon TC. 2000. Nonaqueous phase liquid dissolution in porous media: current state of knowledge and research needs. *Transport in Porous Media* 38:3-28
- Miller CT, Poirier-McNeil MM, Mayer AS. 1990. Dissolution of trapped nonaqueous phase liquids: mass transfer characteristics. *Water Resources Research* 26(11): 2783-2796.
- Powers SE, Abriola LM, Dunkin JS, Weber WJ. 1994. Phenomenological models for transient NAPL-water mass-transfer properties. *Journal of Contaminant Hydrology* 16(1): 1-33.
- Schnaar G, Brusseau ML. 2006. Characterizing pore-scale dissolution of organic immiscible liquid in natural porous media using synchrotron X-ray microtomography. *Environ Sci Technol.* 40(21): 6622-6629.
- Zhang C, Werth CJ, Webb AG. 2002. A magnetic resonance imaging study of dense nonaqueous phase liquid dissolution from angular porous media. *Environ Sci Technol* 36(15):3310-3317.